Top Catal (2014) 57:1171–1187
DOI 10.1007/s11244-014-0284-6

ORIGINAL PAPER

The Reduction-Coupled Oxo Activation (ROA) Mechanism Responsible for the Catalytic Selective Activation and Functionalization of *n*-Butane to Maleic Anhydride by Vanadium Phosphate Oxide

Mu-Jeng Cheng · William A. Goddard III · Ross Fu

Published online: 19 July 2014

Abstract We report here the results of density functional theory quantum mechanical (QM) studies of the detailed chemical mechanism underlying the *n*-butane selective oxidation to form maleic anhydride (MA) on vanadyl pyrophosphate [$(VO)_2P_2O_7$] and vanadyl phosphate [$VOPO_4$] surfaces. This QM-derived mechanism differs substantially from previous suggestions but is in excellent agreement with key experimental observations. We find that the O(1)=P bond of the oxidized X1 phase of the $VOPO_4$ surface is the active site for initiating the VPO chemistry, by extracting the H from the *n*-butane C–H bond. This contrasts sharply with previous suggestions, all of which involved the V=O bonds. The ability of O(1)=P to cleave alkane C–H bonds arises from a new unique mechanism that decouples the proton transfer and electron transfer components of this H atom transfer reaction. We find that the juxtaposition of a highly reducible V^{+5} next to the P=O bond but coupled via a bridging oxygen dramatically enhances the activity of the P=O bond to extract the proton from an alkane, while simultaneously transferring the electron to the V to form V^{+4}. This Reduction-Coupled Oxo Activation (ROA) mechanism had not been known prior to these QM studies, but we believe that it may lead to a new strategy in designing selective catalysts for alkane activation and functionalization, and indeed it may be responsible for the selective oxidation by a number of known mixed metal oxide catalysts. To demonstrate the viability of this new ROA mechanism, we examine step by step the full sequence of reactions from *n*-butane to MA via two independent pathways. We that find that every step is plausible, with a highest reaction barrier of 21.7 kcal/mol.

Keywords Density functional theory · Quantum mechanics · PBE · VOPO · VPO · Vanadium pyrophosphate · $(VO)_2P_2O_7$ · $VOPO_4$

1 Introduction

Vanadium phosphorus oxide (VPO) is a unique catalyst that converts *n*-butane to maleic anhydride (MA) with high selectivity (60–70 %) [1–3]. The partial oxidation of *n*-butane to MA over VPO (Fig. 1) is perhaps the most unique and mysterious heterogeneous catalytic process known. This very deep selective oxidation process involves 14 electrons and yet leads to 65 % selectivity despite what must be a very complex and structure-sensitive mechanism. It is quite successful commercially with several companies providing highly tuned catalysts that deliver this selectivity for years before replacement. This catalyst is responsible for the production of 500 kilotons of MA annually [1] that is used as a feedstock to synthesize numerous valuable products. Indeed, this is the most spectacular application of alkane selective oxidation by a heterogeneous gas–solid

This talk is dedicated to Robert Karl Grasselli, who in 1979 introduced me to the wonderful world of mixed metal (amm)oxidation catalysts. He and the excellent group he put together at SOHIO provided the experiments that yielded key mechanistic information that stimulated our theory and computation studies. Bob is an inspiration to us with his deep thinking and encyclopedic knowledge, all aimed at furthering the science of catalysis. His enormous contributions to heterogeneous catalysis have had a dramatic impact on industry and on the chemical concepts underlying selective oxidation catalysis. I want also to thank Jerry Ebner and John Gleaves for their amazing discoveries made at Monsanto back when it was a leading catalysis innovator, and for the deep insights into the mechanism from their TAP reactor studies.

M.-J. Cheng · W. A. Goddard III (✉) · R. Fu
Materials and Process Simulation Center (139-74), California Institute of Technology, Pasadena, CA 91125, USA
e-mail: wag@wag.caltech.edu

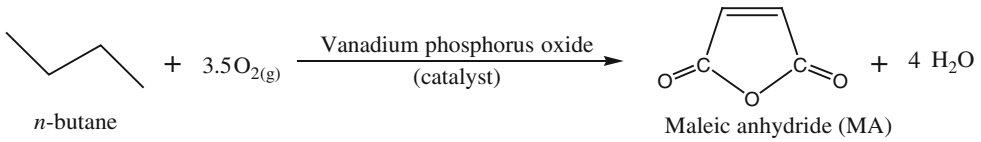

Fig. 1 The VPO catalyst leads to spectacularly high selectivity (65 % selectivity with 80 % conversion at 650 K) for the very deep partial oxidation of *n*-butane to maleic anhydride

catalytic process. Thus, improving the yield of MA from the current value of 50 % [1] would bring enormous economic and environmental benefits [2]. A major impediment in improving this system is the lack of atomistic level reaction mechanisms to focus attention on the atomistic origins of the critical barriers for the selective and nonselective processes. In this article we report this mechanism.

The most active phase has been identified as vanadyl pyrophosphate, $(VO)_2P_2O_7$ (denoted VOPO) [1]. Numerous experimental [1–3] and a few theoretical [4–9] studies have been directed toward understanding the reaction mechanism underlying this remarkable system, but no one has yet suggested a plausible mechanism. Insights that have been obtained include the following:

Gleaves et al. [10] established a reaction network using a TAP (temporal analysis of products) microreactor, proposing that *n*-butane is first oxidized to butenes, then consecutively to 1,3-butadiene, furan, and finally to MA. Of particular interest is the discovery that pre-dosing with enough O_2 and then exposing the catalyst to doses of *n*-butane lead only to MA (no partially oxidized intermediates), suggesting that the reaction may be completed on a *single* active site. In contrast, with lower O_2 doses, highly reactive intermediates such as butenes and butadiene are desorbed, lowering the selectivity [10, 11]. Thus, Gleaves suggested that the oxidation follows an olefinic route [10], during which reaction intermediates desorb and readsorb to complete the reaction.

Others suggest that the reaction follows an alkoxide route mechanism [12, 13], in which *n*-butane anchors on the surface after the initial C–H activation and desorbs only when the final product MA is formed. This would explain the lack of partially oxidized intermediates under conditions of a working catalyst.

Coulston et al. [14] showed that a small amount of V^{+5} is crucial for a successful catalyst, based on in situ X-ray absorption spectroscopy studies.

Besides the uncertainty in the mechanism, essentially all the basic questions remain unanswered. It is even unknown which sites on the surface do the initial C–H bond cleavage from *n*-butane [3, 15].

2 Computational Details

2.1 DFT Calculations

We performed density functional theory (DFT) calculations with periodic boundary conditions using the Perdew–Burke–Ernzerhof (PBE) functional [16], as implemented in the Quantum Espresso code. We used ultrasoft pseudopotentials (USPPs) [17] with a planewave basis set and a cutoff energy of 30 Ry for wavefunctions and 240 Ry for charge density. We used the Gaussian electron-smearing technique with a width of 0.01 Ry.

For bulk structures, the Brillouin zone was sampled with $3 \times 3 \times 4$ Monkhorst–Pack *k*-point grid [18] for α_I- and α_{II}-$VOPO_4$, and $2 \times 2 \times 2$ for β-, δ- and X1-$VOPO_4$ and $(VO)_2P_2O_7$. For slab calculations, the Brillouin zone was sampled with $3 \times 3 \times 1$ *k*-point net for α_I- and α_{II}-$VOPO_4$ surfaces, and $2 \times 2 \times 1$ for X1-$VOPO_4$ and $(VO)_2P_2O_7$ surfaces. About 8 Å of vacuum space between adjacent slabs was used to prevent the interaction between the replicas along the *z* direction.

Transition states were located by using the "climbing-images" nudged elastic band (CI-NEB) method [19, 20]. Most calculations used the spin-polarized wavefunction in which the up-spin orbitals are allowed to be different from down-spin. The exceptions are the calculations of the total energies of the various phases of $VOPO_4$. We also performed some calculations using the VASP code with the same k-point net to sample the reciprocal space, projector augmented-wave (PAW) pseudopotentials, and the setting PREC = ACCURATE. We calculated the binding energy between the surface oxygen to a hydrogen atom to be 49.9, 50.8, 52.1, 45.2, and 82.4 kcal/mol for O(1) and O(2) on the α_I-$VOPO_4$ surface, and O(1) and O(2) on the α_{II}-$VOPO_4$ surface, and O(1)=P on the X1-$VOPO_4$, respectively. These numbers are similar to those obtained by the Quantum Espresso code with USPPs (48.5, 49.2, 52.1, 45.2, and 84.3 kcal/mol). This indicates that the use of USPPs gives essentially the same results as the use of PAW.

In order to reduce the computational cost, we used the high pressure, high symmetry form of $(VO)_2P_2O_7$ [21], which has four molecular units per unit cell as compared to the ambient pressure, low symmetry form with eight units [22]. We found that the band structures, projected density

of states, and Mulliken charge distributions are very similar for the two forms, and hence we expect the surface chemistry to be similar [4].

As discussed below, we find that all reactions with the C–H bonds of *n*-butane involve the O(1)=P active site. Thus we calculated the binding energy (D_H) of a free hydrogen atom to O(1)=P using the low symmetry, ambient pressure form of oxidized VOPO (X1-$VOPO_4$) and compared the result to that using the high symmetry, high pressure form of oxidized VOPO. We found the two D_H's are quite similar (86.1 vs. 84.3 kcal/mol). As a result, we expect that the results based on the high symmetry form are similar to those that would be obtained using the low symmetry model.

Optimization of the cell parameters of $(VO)_2P_2O_7$ (0 K) with the PBE functional leads to $a = 7.624$ Å, $b = 9.661$ Å, and $c = 8.445$ Å, in good agreement with experiment ($a = 7.571$ Å, $b = 9.536$ Å, and $c = 8.362$ Å at 300 K) with deviations of 0.7, 1.3, and 1.0 %, respectively [21]. Since the atoms within the layers on the *bc* plane connect to adjacent *bc* layers through interlayer P–O–P bonds along the *a* direction, we expected that London dispersion (van der Waals attraction) might play an important role. Therefore, we re-optimized the cell parameters with dispersion-corrected PBE (PBE-D2) functional [23] to obtain $a = 7.447$ Å, $b = 9.558$ Å, and $c = 8.446$ Å, which deviate from the experimental values by −1.6, 0.2, and 1.0 %, respectively. Thus PBE-D2 does reduce the error in the calculated cell volume while the error in the *a* parameter goes from +1.0 to −1.6 %. We also re-calculated the binding energy of atomic hydrogen to O(1)=P (which we identify as the active site for the VPO chemistry) using PBE-D2 (with a surface model taken from the PBE-optimized unit cell), leading to 87.5 kcal/mol for PBE-D2 compared to 84.3 kcal/mol for PBE. Thus, we conclude that the results from PBE are similar to those based on PBE-D2.

For small finite clusters, geometry optimizations were carried out using the same PBE functional as implemented in the Jaguar code. We used the 6-31G** basis set [24, 25] for all atoms except V. For V, the Ne shell of core electrons was described using the small core Los Alamos angular momentum projected effective core potential with the double-ζ contraction of valence functions (denoted as LACVP**) [26–31].

We carried out a full optimization of the VOPO bulk structure (Figs. 2, 3), including atomic positions and cell parameters under orthorhombic symmetry. The VOPO surface model used in this work was prepared by cutting the DFT-optimized bulk structure parallel to the *bc*-plane, cleaving the P–O–P interlayer bonds. It is generally agreed that the active sites involved in *n*-butane oxidation to MA are on this surface [1, 32]. We capped the cleaved sites with either hydrogen atoms or hydroxyl groups so that vanadium and phosphorus are maintained at the +4 and +5 oxidation state, respectively, while keeping the surface unit cell neutral. The total number of atoms in the unit cell is 58, which includes eight vanadium, eight phosphorus, four OH, and 34 oxygen atoms. Saturating the cleaved P–O bonds in this way is reasonable since Busca et al. [32, 33] observed that such P–OH motifs exist on the VOPO surface with vibrational frequencies of 2,600 to 3,600 cm^{-1}.

2.2 QM Results on Bulk Properties of $(VO)_2P_2O_7$

Hints regarding the reactivity of VOPO were provided by our recent study of its low-temperature magnetic structure

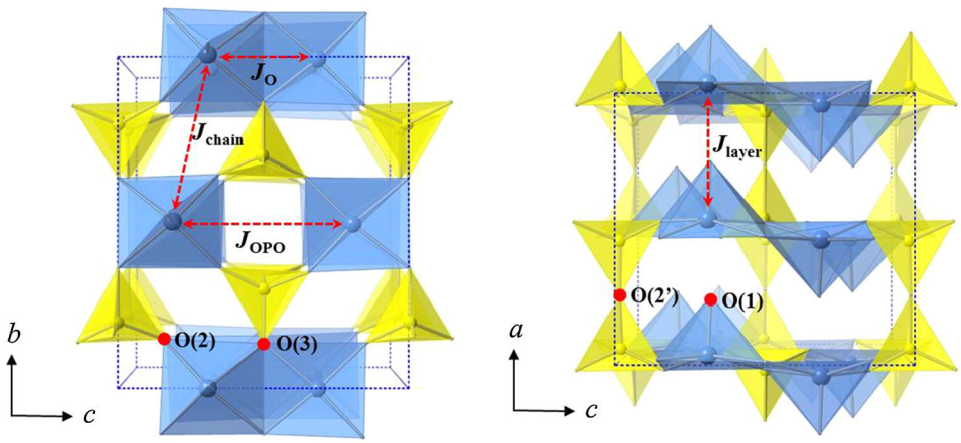

Fig. 2 *Top* and *side view* of high pressure, high symmetry form of $(VO)_2P_2O_7$. Each V is in the IV oxidation state with a singly occupied *d*-orbital. The four different types of spin coupling interactions between these *d*-electrons are indicated. The J_{OPO} along the chain but across the 8 membered ring is the strongest (antiferromagnetic) coupling. The J_O along the chain but across the 4 membered ring is weakly antiferromagnetic at the equilibrium geometry, but becomes weakly ferromagnetic upon compression by 5 %. The interchain and interlayer couplings are very weak and ferromagnetic

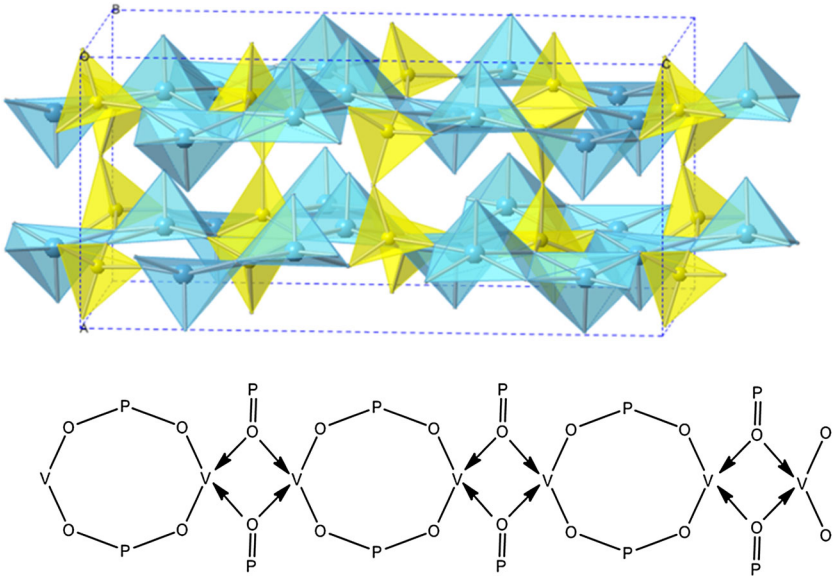

Fig. 3 Valence bond description of the $(VO)_2P_2O_7$ crystal. Note that each P shown here has three P–O single bonds that bridge to two neighboring V atoms and a neighboring P atom. Thus, the bond of the P=O oxygen with the V in the four-membered ring is a dative donor–acceptor bond, leaving this unit very flexible. Each V shown here has also a V=O bond out of the plane, leading to a IV oxidation state with a singly occupied *d* orbital remaining on the V

[4]. The S = ½ V^{+4} centers couple magnetically (1) to the other site within the dimer, J_O, (2) to the nearest site in the next dimer in the chain, J_{OPO}, (3) to the site in the chain above J_{layer}, and (4) to sites in the parallel chains, J_{chain} (Fig. 2). By evaluating the energies of many spin configurations (ferro- and antiferromagnetically coupled neighbors) with B3LYP DFT and periodic models, we were able to fit coupling parameters [4]. Two large couplings exist along the chain direction (*c*-axis), which we predict to be $J_{OPO} = -156.8$ K and $J_O = -68.6$ K. For the two weaker couplings appear along the *a* (between two layers) and *b* directions (between two chains in the same layer), we calculate the couplings to be $J_{layer} = 19.2$ K and $J_{chain} = 2.8$ K, which is weakly ferromagnetic.

We found that stretching or compressing the chain has little effect on J_{OPO} but has a dramatic effect on J_O, changing it to ferromagnetic upon just 5 % distortion. This indicates that the bonds of the V–$(O)_2$–V unit are fragile and dative. This is because these oxygen atoms are double bonded to the P, so that there are no electrons left to bond to the V [4]. We estimate that breaking apart the vanadyl dimers at the surface costs only ~9 kcal/mol (based on a cluster model).

We also carried out by 2-D periodic quantum mechanical (QM) models of the (002) VOPO surface, in which we found that the vanadyl groups stacked in the *c* direction communicate with one another [34]. Thus, after oxidizing the top V from +4 to +5, the V^{+4} site in the second layer can transfer its electron to the surface while forming a covalent bond to the oxygen that is now shared by the two new V^{+5} sites. This coupling had been suggested for VOPO by Goddard in [9]. We also observed this process in ReaxFF reactive molecular dynamics studies of the dehydrogenation of CH_3OH by V_2O_5, where formation of the product H_2O was trapped at a V^{+3} site until the V=O bond of the subsite bridged to the top site to form two V^{+4} bridged by an O atom [35].

2.3 The H Atom Surrogate Shortcut for Assessing Surface Reactivity

We are interested in assessing which surface sites (SS) can activate butane. We find that the reaction is generally endothermic with a linear transition state SS–H–butyl and a barrier that is generally ~5 to 10 kcal/mol greater than the endothermicity. Thus, writing the butyl-H bond energy as D_{C-H} and the bond energy of H to SS as D_{SS-H}, the overall barrier is

$$E_{barrier} = \delta + (D_{C-H} - D_{SS-H})$$

where δ ~5 to 10 kcal/mol and $D_{C-H} = 100$ kcal/mol (for the secondary C–H bonds of butane). Since $\delta + D_{C-H}$ ~105 to 110 kcal/mol is independent of the SS, we can search over all potential SSs, examining just the energy of bonding an H atom. For the VPO catalysts, various experiments estimate that the activation barrier is $E_a = 12.9$ to 23.6 kcal/mol, depending on the degree of oxidation of VPO [11]. Thus, we can limit our search to SSs that have a bond energy of $D_{SS-H} = 81$ to 97 kcal/mol.

3 Results

3.1 The Reduced Structure, $(VO)_2P_2O_7$

The starting structure for the $(VO)_2P_2O_7$ catalysts has been well characterized. As shown in Figs. 2 and 3, it has chains of V sites connected by O atoms shared with phosphates,

plus a vanadium oxo bond, V=O, perpendicular to the sheet. This V has oxidation state +4, so that there is a d_{xy} singly occupied orbital on each V, which is antiferromagnetically coupled to its neighbors.

As shown in Fig. 4, we calculated the bond energy of a free hydrogen atom to the O(1)=V (vanadyl) group to be $D_{O(1)–H}$=58.2 kcal/mol, so that the activation energy is expected to be ~47 kcal/mol, far too high to explain the experimental data. We also examined the O bridging between V and P, which we found leads to $D_{O(2)–H}$ = 17 kcal/mol, extremely inactive as expected.

Thus we can conclude that neither the V=O bond or the V–O–P bond of the reduced structure, $(VO)_2P_2O_7$, can be responsible for activating *n*-butane.

There have been other proposals for the reactivity. For example, it has been proposed that gaseous O_2 may adsorb on the VOPO surface as a peroxyl radical or dissociatively, oxidizing V^{+4} to V^{+5} to form very reactive oxygen species in the form of O^-, O_2^-, or O_2 [15, 36, 37], as in Fig. 5. However we found that the binding of O_2 to the VOPO surface is uphill by 2.8 kcal/mol (electronic energy) rather than downhill (Fig. 5a), even though two V^{+4} are oxidized to V^{+5}. Moreover, we find that gaseous O_2 chemisorbed to the vanadium, led to a D_H from the oxygen of peroxyl of 70.0 kcal/mol, indicating that the C–H activation barrier would be at least 35 kcal/mol.

We also considered the dissociative adsorption of O_2 (g) onto the VOPO surface. As described in [9], we added two oxygen atoms to the top of vanadium (the position *trans* to O(1)). Geometry optimization leads to the formation of two new O=V bonds but simultaneously pushes the two original O(1) atoms to bind with V=O(1) on the second layer, forming two *trans*-vanadium dioxo motifs (O(1)–V–O(1), (b)) on the other side of the surface. Here, Lowdin spin density analysis shows that the two newly added oxygen atoms possess some radical character (0.15 e^-),

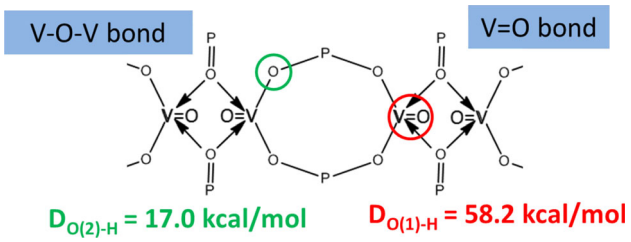

Fig. 4 O–H bond strength for oxygen atoms on the $(VO)_2P_2O_7$ surface. The minimum energy barrier for O(1) to activate *n*-butane is ~47 kcal/mol and hence neither of these oxygens can be responsible for the observed activation of *n*-butane. Thus, the unoxidized catalyst, $(VO)_2P_2O_7$, cannot be responsible for the observed activation of *n*-butane, and we must look for an oxidized form. We tried to calculate the bond energy for H to attach to the O(3) bond at the P=O site, but after geometry optimization the added hydrogen was transferred to the nearby –P–O(2)–P– (the *green* one)

but they lead to $D_{SS–H}$ = 58.9 kcal/mol, far too weak to explain the observed activation.

These results indicate clearly that neither the oxygen on the VOPO surface nor adsorbed O_2 (molecularly or dissociatively) is the active site for initial *n*-butane C–H activation. From experimental studies of the same oxidation reaction catalyzed on supported vanadia, Wachs et al. [38, 39] reached the same conclusion. Thus we conclude that the reduced form of the VPO catalyst is not the active catalyst.

3.2 The Oxidized Surface $VOPO_4$

Experiments show that the surface of the working VPO catalyst contains small amounts of various phases of $VOPO_4$ as in Fig. 6. [40, 41] This opens a possibility that V^{+5}, which is known to activate alkanes and furan [14], may come from the surface of $VOPO_4$. There are five known phases of $VOPO_4$, with calculated energies as in Fig. 7.

Comparing the structures of these well-defined $VOPO_4$ structures (α_I, α_{II}, δ, and β phases) to VOPO, we see no significant structural change at the V atoms. Instead, the major changes are at phosphorus (Fig. 8). In VOPO, each

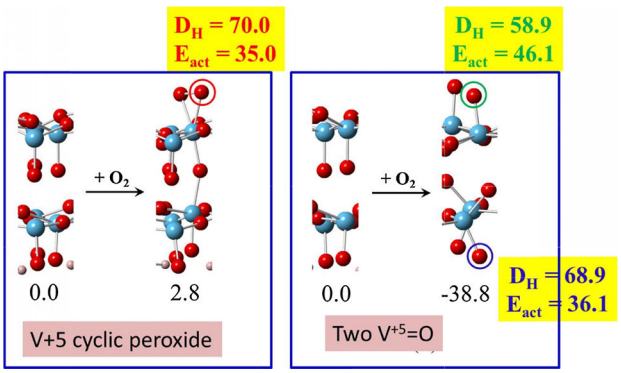

Fig. 5 Oxygen adsorption energies on the $(VO)_2P_2O_7$ surface and the O–H bond strength (D_H) to each of these O atoms, along with the lower bound on the activation energy (E_a) for *n*-butane C–H cleavage (*colored numbers*, energies in kcal/mol). According to our results, both of these mechanisms lead to reaction barriers too large to account for the observed activation of *n*-butane

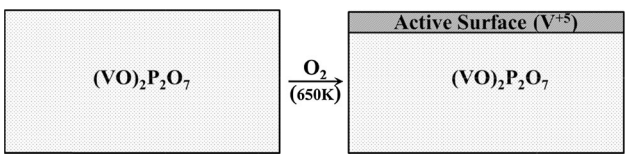

Fig. 6 Oxidation of $(VO)_2P_2O_7$ leads to the formation of $VOPO_4$ on the surface layers

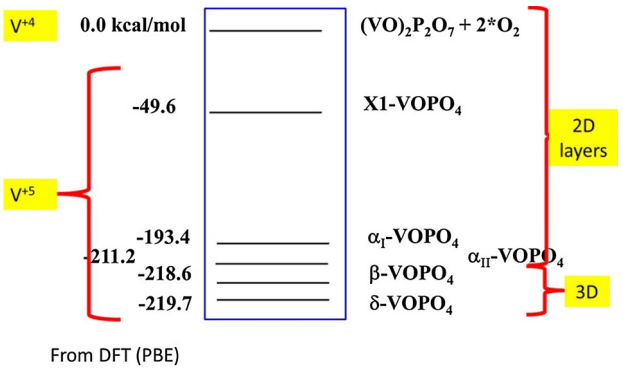

Fig. 7 Phase stability (kcal/mol) of various phases of $VOPO_4$ (referenced to $(VO)_2P_2O_7 + O_2$). From PBE DFT calculations

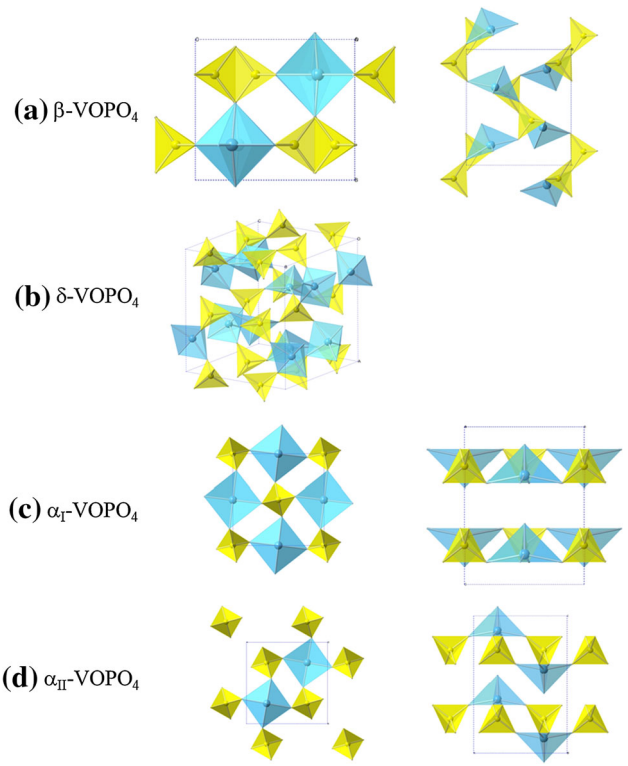

Fig. 8 3D structures for β-, δ-, α_I, and α_{II}-$VOPO_4$. As indicated, α_I and α_{II} are layered with V=O bonds but not P=O bonds. The β and δ phases do not lead to layers and also have no P=O bonds. The β and δ phases do have V=O(1) bonds, but we did not calculate O–H bond strengths to them. This is because they have 3-D structures without obvious layers to serve as the catalyst surface under catalyst operational conditions. As discussed in the text, the charge on the V=O in both the β and δ phases is similar to that of the α_I and α_{II} phases, so we consider that the results would be the same

phosphorus atom forms one O–P bond (the pyrophosphate P–O–P bond that links two adjacent layers) and four O–V bonds, whereas in $VOPO_4$ phosphorus binds with four O–V motifs.

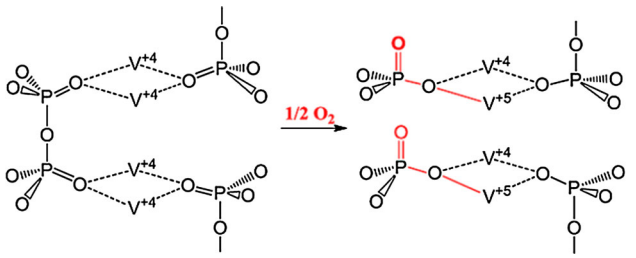

Fig. 9 Valence bond description of pyrophosphate oxidation to phosphate. (O(1)'s on vanadium are omitted for clarity)

This suggests that the oxidation of VOPO to $VOPO_4$ may occur by adding oxygen to phosphorus, converting one pyrophosphate into two orthophosphates (Fig. 9). In this way, two of the dative bonds in the V–$(O)_2$–V motif of VOPO become covalent, and concurrently two V^{+4} are oxidized to V^{+5} [4, 34]. This increase in the oxidation state for vanadium may enhance the reactivity of the surface oxygen toward *n*-butane C–H activation.

In order to verify this hypothesis, we studied bulk $VOPO_4$ and the corresponding surfaces. We first optimized the cell parameters and atomic positions of these $VOPO_4$ phases under orthorhombic symmetry. The relative energies of these phases are shown in Fig. 7 (from PBE DFT calculations).

3.2.1 *The α_I, and α_{II} Phases of $VOPO_4$*

The α_I and α_{II} phases lead to layered structures and are nearly as stable as β and δ. For the DFT calculations we prepared the surfaces by cleaving parallel to the layer direction in such a way that only van der Waals bonds are broken.

The results are shown in Fig. 10. For the α_I-surface, we find $D_{O(1)–H} = 49.2$ and $D_{O(2)–H} = 48.5$ kcal/mol, far too weak to activate *n*-butane.

For the α_{II}-surface, we find $D_{O(1)–H} = 52.1$ and $D_{O(2)–H} = 45.2$ kcal/mol, also far too weak to activate *n*-butane.

This indicates clearly that none of the vanadium oxygen sites on the α_I- or α_{II}-surfaces can be the reactive center for VPO chemistry.

3.2.2 *The β and δ Phases of $VOPO_4$*

The β and δ phases are the most stable phases, but as shown in Fig. 8, they do not lead to layers that could form stable surfaces for the reactions. We did not calculate the O–H bond strength for β- and δ-$VOPO_4$, because they do not have layered structures, making it difficult to decide which surface is the most stable and how to saturate the surface (remove broken bonds). These structures do not

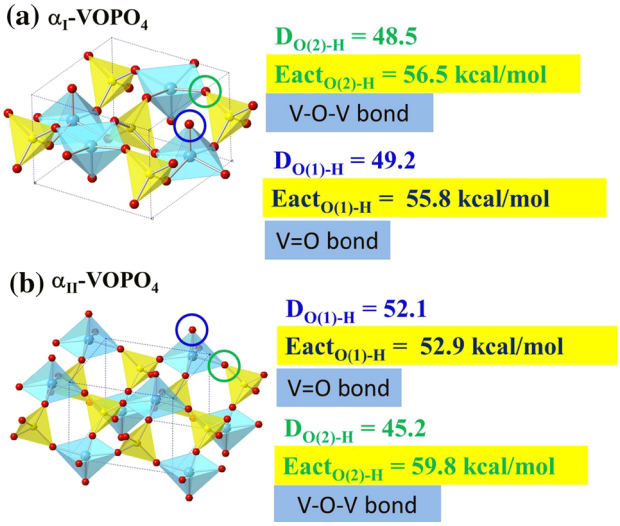

Fig. 10 O–H bond strength for oxygen bonded to V atoms on the α_I- and α_{II}-$VOPO_4$ surfaces, and the corresponding lower bound on the activation for *n*-butane C–H cleavage. None of these oxygen atoms can be responsible for the observed activation of *n*-butane

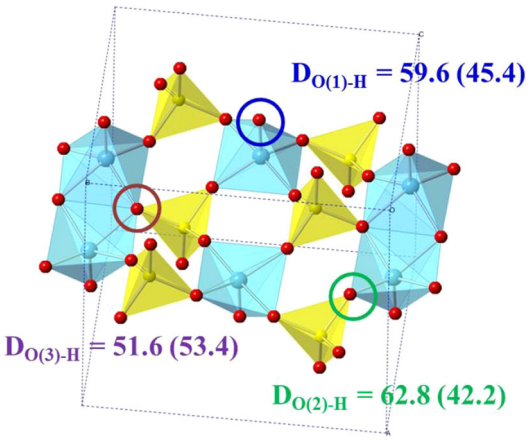

Fig. 11 O–H bond strength to oxygens on the X1-$VOPO_4$ surface that are bonded to vanadium. Each number in parentheses is the lower bound on the activation for *n*-butane C–H cleavage. None of these oxygens can be responsible for the observed activation of butane

lead to P=O bonds. Instead, each P is connected through O to four vanadium atoms. However, we did calculate the vanadium 3*s* core orbital energy (chemical shift) for bulk β-$VOPO_4$ and compared it to those from α_I- and α_{II}-$VOPO_4$ (using B3LYP/Crystal). We found the 3*s* core orbital energies and net charge on the O(1) to be similar, and hence we expect their O–H bond strengths to be similar.

3.2.3 The X1 Phase of $VOPO_4$

Having eliminated the β, δ, α_I- and α_{II}-surfaces, we turned to the X1 phase [42] despite it being much less stable. The results are shown in Fig. 11, in which we see that $D_{O(1)–H} = 59.6$, $D_{O(2)–H} = 62.8$ and $D_{O(2)–H} = 51.6$ kcal/mol. Thus, none of the V–O bonds on the X1 phase can be responsible for activating *n*-butane.

To summarize, we have now examined the reduced surface $(VO)P_2O_7$ and the surfaces of all five known phases of the oxidized form $VOPO_4$, and found that none has a surface V–O site capable of activating *n*-butane. Yet the experiments show that there must be a site that can do this and it must lead to bond of at least $D_{SS–H} = 81.0$ kcal/mol. What can the answer be?

3.2.4 The P=O Bond and the Reduction-Coupled Oxo Activation (ROA) Mechanism

Here we took a lesson from Sherlock Holmes: "Eliminate all other factors, and the one which remains must be the truth" (from *The Sign of Four*, Chapter 1: "The Science of Deduction"). Also: "…when you have eliminated the impossible, whatever remains, however improbable, must be the truth" (from *The Sign of Four,* Chapter 6: "Sherlock Holmes Gives a Demonstration").

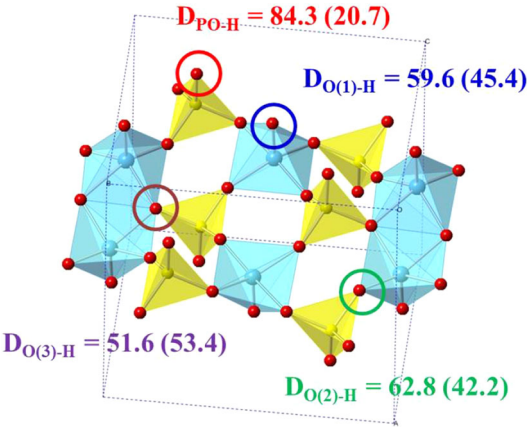

Fig. 12 O–H bond strengths for oxygen on the X1-$VOPO_4$ surface, but now including the possibility of bonding to the P=O bond. Each number in parentheses is the corresponding lower bound on the activation for *n*-butane C–H cleavage. The O–H bond strength of 84.3 kcal/mol to the P=O bond leads to an estimated activation energy of 20.7 kcal/mol, which is the first candidate site whose activation energy is compatible with experiment

The only factor we had not considered was the P=O bond. This is clearly improbable since no one had ever before considered it. The results are shown on Fig. 12, where we find that $D_{PO(1)–H} = 84.3$ kcal/mol! Finally, we have a sufficiently active site, but oh so improbable! P=O

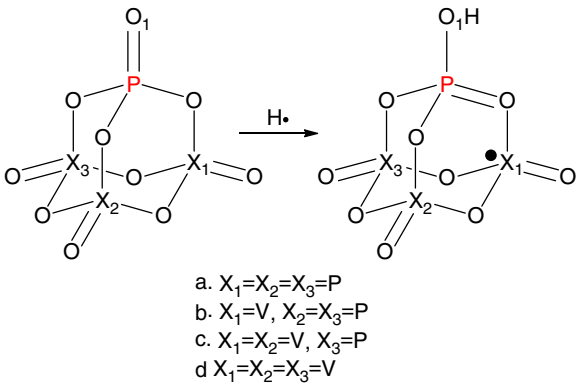

Species	$D_{P(O1)-H}$
a. P_4O_{10}	28.2
b. P_3VO_{10}	60.5
c. $P_2V_2O_{10}$	84.3
d. PV_3O_{10}	89.2

Fig. 13 Use of finite cluster models to investigate how the O–H bond strength (kcal/mol) of P=O bonds depends on the number of V that connected to the P via O linkages. This indicates that a single linkage to V makes the PO bond 32.3 kcal/mol more active, while coupling to a second vanadium makes it an additional 23.8 kcal/mol more active and coupling to a third V (as in VPO) makes it an additional 4.9 kcal/mol more active

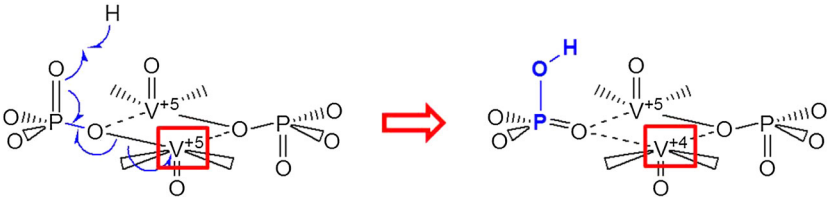

Fig. 14 Valence bond description of the hydrogen abstraction process by P=O. This illustrates the new ROA reaction mechanism

bonds are normally far less reactive. For example, for P_4O_{10} (Fig. 13a) we calculate $D_{PO(1)-H} = 28.2$ kcal/mol. In contrast, replacing an adjacent P=O with V=O increases the P=O bond to $D_{PO(1)-H} = 60.5$ kcal/mol (b).

The principle underlying the remarkable ability of the P=O bond of the X1 phase of $VOPO_4$ to active *n*-butane is shown in Fig. 14.

Here, the P is initially P^{+5} with one P=O bond and three single bonds bridging to two adjacent V atoms and one adjacent P. Also, the V^{+5} has one V=O bond with three electrons shared between the remaining four bonds to the four O atoms that bridge to the other P or V. Since this V started with five valence electrons, the valence bond view is that there are three covalent V–O bonds and one donor–acceptor V ← :O bond.

Reacting the H to the P=O leads to P–O–H, but instead of this leaving an unpaired spin on a P^{+4}, the P now forms a P=O bond to one of the V, remaining P^{+5}.

This converts what had been a V–O–P unit with single bonds to both V and P to V···O=P with a donor acceptor bond to the V, leaving the V with an extra electron in the d_{xy} orbital, and hence V^{+4}.

It is the ability of the V^{+5} to accept this electron that makes the $D_{PO(1)-H}$ bond so strong.

Indeed, the spin analysis after bonding the H to P=O of the X1 phase shows 0.61 e on one neighboring V and 0.45 e on the other (Fig. 15).

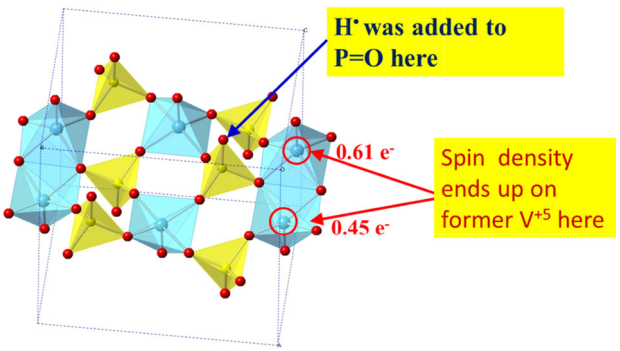

Fig. 15 Spin density analysis shows that the electron and proton from hydrogen atom abstracted from butane are decoupled. The proton binds with O=P, whereas the electron is transferred to vanadium (in this case partially on two vanadium atoms)

Figure 16 shows the transition state calculated for activating *n*-butane by P=O on the X1-$VOPO_4$ surface. We find an activation energy of 13.6 kcal/mol, which is consistent with the range of experimental results of 12.9–23.6 kcal/mol [11, 43].

Thus we propose that O(1)=P on the metastable X_1-$VOPO_4$ surface is the active center for initiating the VPO chemistry. This conclusion is in stark contrast to the common assumption that pyrophosphate or phosphate is a linking ligand and catalytically inactive.

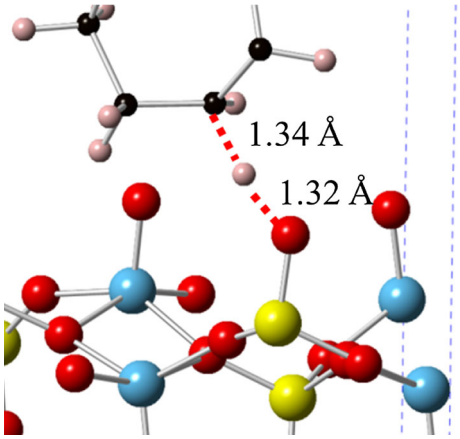

Fig. 16 Transition state structure for the first *n*-butane C–H cleavage by O=P. The calculated activation barrier is 13.6 kcal/mol. We were surprised that this is not 5–10 kcal/mol higher than the minimum estimated barrier of 13.7 kcal/mol, based on the isolated product (surface-H + C_4H_9) [50]. We speculate that charge transfer between the substrate and the surface may stabilize the transition state to reduce the barrier

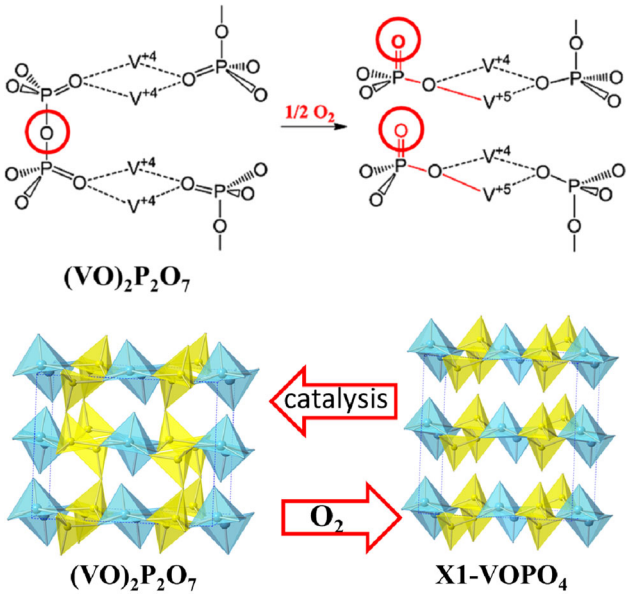

Fig. 17 Direct oxidation of $(V^{+4}O)_2P_2O_7$ by O_2 involves oxidizing one P_2O_7 to two PO_4, leading directly to the X1-$V^{+5}OPO_4$ phase

Our conclusion is in contrast to all previous speculations of the mechanism based on experimental [3, 15] and theoretical studies [4–9], which suggested that the reactive center is either a V–O bond [3] or chemisorbed O_2 on vanadium [15].

3.2.5 *Plausibility of the X1 Phase as the Catalytically Significant Phase*

Although we have now shown that the P=O bond of the X1 phase can activate *n*-butane, we still have an important issue to settle. Why should we expect the catalyst to remain in the X1 phase when the other four phases of $VOPO_4$ are much more stable?

Our explanation is illustrated in Fig. 17. We visualize that the chemistry (reduction and oxidation) is proceeding rapidly in the top few layers, where X1 regions catalyze conversion of *n*-butane to MA while simultaneously reducing the local region toward the reduced form $(VO)_2P_2O_7$, which in turn later gets reoxidized by O_2 to form the X1 phase. Thus, at some times parts of the top few layers are reduced and coupled via pyrophosphate bonds while at other times they are oxidized and separated, allowing them to react with *n*-butane. It is plausible to us that this dynamic equilibrium with constant interconversion between $(VO)_2P_2O_7$ and X1-$VOPO_4$ would maintain the oxidized form in the X1 phase because massive atomic rearrangements would be necessary to convert to the other phases of $VOPO_4$. We expect that such conversion of X1 into these other phases would lead to catalyst deactivation, requiring a more massive reduction to convert back to $(VO)_2P_2O_7$, which may be reoxidized by O_2 to X1 and then continue the selective catalysis.

3.2.6 *Demonstration that the X1 Phase Can Continue to Complete the Many Reaction Steps to Form MA Product without High Activation Barriers: The Olefinic Route Mechanism*

To demonstrate that our proposed highly reactive surface of X1-$VOPO_4$ is able to convert *n*-butane all the way to MA, we studied the subsequent steps of this oxidation reaction, considering two mechanisms proposed in the literature (Fig. 18):

> The olefinic route mechanism, in which *n*-butane is first converted to butene, butadiene, dihydrofuran, crotonlactone, and finally MA [10, 44]. The mechanism was established for low pressure conditions by Gleaves [10] using a TAP reactor to determine the intermediates desorbing to the gas phase.
> The alkoxide route mechanism [12], in which the intermediates stay on the surface without desorbing into the gas phase. This mechanism is consistent with the high selectivity observed in practice, with little gas phase intermediates observed.

In this section we consider the olefinic route mechanism using a one-layer computational model for the QM calculations. The results are summarized in Fig. 19. Here we will go through these steps one by one. The numbering in this figure goes down from a to e, and we refer to the columns as 1, 2, 3, and 4.

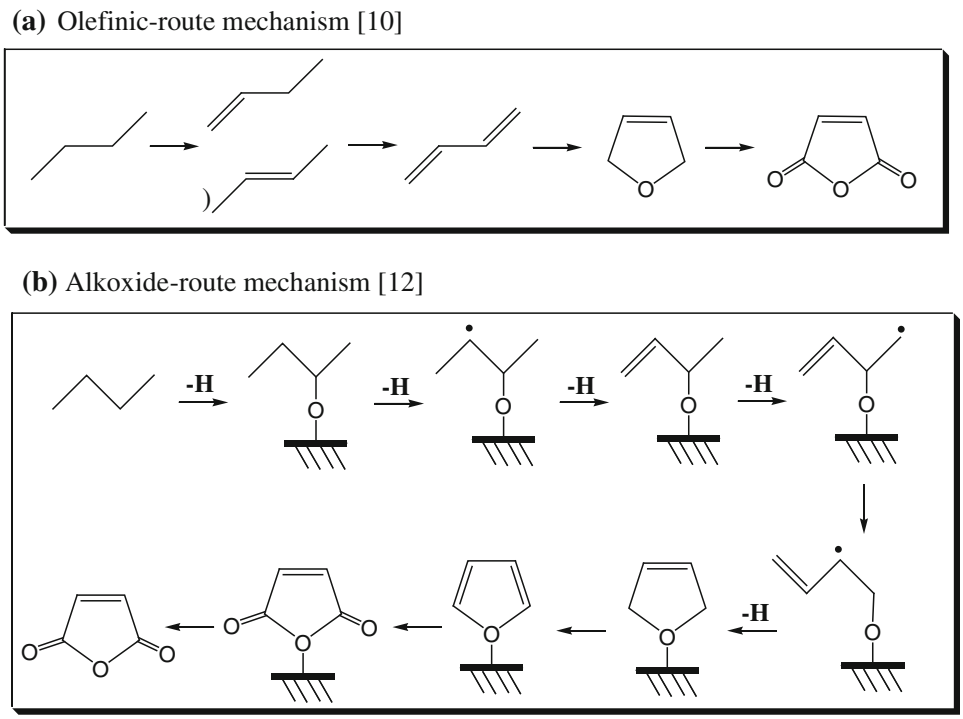

Fig. 18 Two proposed mechanisms for VPO-catalyzed *n*-butane oxidation to maleic anhydride. **a** Olefinic-route mechanism [10]. **b** Alkoxide-route mechanism [12]

- *Step a12* Activate secondary C–H bond of *n*-butane by P=O. This has $E_a = 13.6$ kcal/mol and $\Delta H = -0.6$ kcal/mol and is thus thermoneutral.
- *Step a23* Trap butyl radical onto a V=O bond. This has $\Delta H = -21.3$ kcal/mol and we assume no enthalpic barrier.
- *Step a34* Use a second P=O to extract H from the remaining secondary C to form 2-butene, while reforming the V=O bond. This has $E_a = 14.7$ kcal/mol and $\Delta H = -4.0$ kcal/mol.
- *Step b12* Use a third P=O to activate 2-butene to form butenyl radical. This has $E_a = 8.1$ kcal/mol and $\Delta H = -3.1$ kcal/mol (includes allylic resonance stabilization).
- *Step b23* Trap butenyl radical on a V=O site. This has $\Delta H = -5.9$ kcal/mol and we assume no enthalpic barrier.
- *Step b34* Extract H from butenyl using a fourth P=O site to form butadiene, releasing the V=O site. This has $E_a = 7.2$ kcal/mol and $\Delta H = -9.9$ kcal/mol (loses allylic resonance stabilization).
- *Step c12* Trap butadiene at a V=O site. This has $E_a = 11.8$ kcal/mol and $\Delta H = +6.3$ kcal/mol (slightly endothermic despite allylic resonance).
- *Step c23* Close ring to form 2,5-dihydro-furan bound to surface at a V site (uses up one V=O site).
- *Step c34 (not shown)* Forming 2,5-dihydro-furan attached to the V=O in step c23 leads to a V^{+3} site that binds quite strongly to the 2,5-dihydro-furan. But it is favorable for the V^{+5}=O bond of the second layer to react with the V^{+3} of the top layer forming V^{+4}–O–V^{+}. This in turn allows the 2,5-dihydrofuran to desorb [35].
- *Step d12* Use a fifth P=O to activate 2,5-dihydrofuran. This has $E_a = 6.4$ kcal/mol and $\Delta H = -20.0$ kcal/mol (includes allylic resonance stabilization).
- *Step d23* Trap 2,5-dihydrofuran radical on a V=O site. This has $\Delta H = -1.6$ kcal/mol and we assume little enthalpic barrier (it loses allylic resonance stabilization).
- *Step d34* Use a sixth P=O to remove H from the α-C, forming 2,5-dihydrofuran-2-one bound to the surface (uses a second V=O site). This has $E_a = 21.7$ kcal/mol and $\Delta H = -12.4$ kcal/mol.
- *Step d45 (not shown)* Step 34 leads to a V^{+3} site. Just as in step c34, the V^{+5}=O of the second layer can interact with the surface V^{3+} to form V^{+4}–O–V^{+4}, allowing the 2,5-dihydrofuran-2-one to desorb [35].
- *Step e12* Use a seventh P=O to extract H from the C of 2,5-dihydrofuran-2-one. This has $E_a = 15.8$ kcal/mol and $\Delta H = +6.5$ kcal/mol.
- *Step e23* Trap the 2,5-dihydrofuran-2-one radical at a V=O site. This has $\Delta H = -16.0$ kcal/mol and we assume little enthalpic barrier (it loses allylic resonance stabilization).
- *Step e34* Use an eighth P=O to extract H from the C to form the product MA (uses third V=O site) still bonded to the surface. This has $E_a = 19.1$ kcal/mol and $\Delta H = -7.1$ kcal/mol.

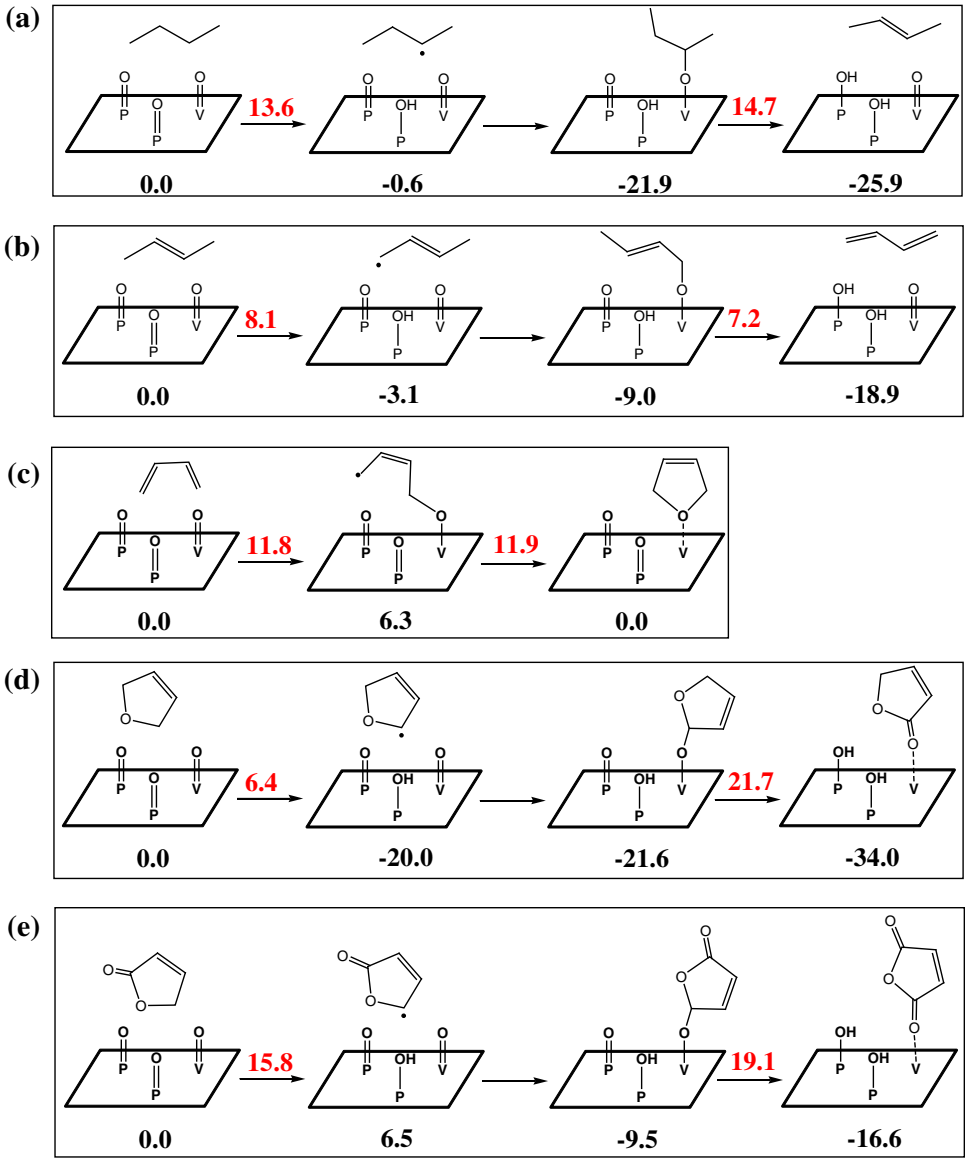

Fig. 19 DFT-PBE calculated potential energy surface based on the olefinic-route mechanism. The activation energies are shown above the *arrows*. Energies in kcal/mol

- *Step e45 (not shown)* As in step c34 and d45, the V^{+5}=O of the second layer can react with the surface V^{+3} sit to form V^{+4}–O–V^{+4}, allowing the MA to desorb [35].

Summarizing the olefinic-route mechanism, we find that the highest barrier in the conversion of *n*-butane to MA is 21.7 kcal/mol, quite consistent with experiment, which leads to E_a = 12.9 to 23.6 kcal/mol [11, 43].

In this reaction sequence, eight surface P=O sites react with the substrate to form eight POH, each reducing one V^{+5}=O to V^{+4}=O. In addition 3V=O sites were converted to V^{+3} which in turn reacted with the subsurface V^{+5}=O to form V^{+4}–O–V^{+4}. Thus the net result is to form 14 V^{+4} sites with three V–O–V pairs coupling between the two layers.

We assume that subsequent reactions with O_2 can recover the oxidized surface states. All steps are consistent with QM and experiment, but there could be other processes as good or better. We should note that our mechanism ends up with eight POH units on the surface, which ultimately lead to $4H_2O$ products, while leaving behind four coupled pyrophosphates. It is possible that these steps may require for operation at 650 K.

3.2.7 *Demonstration That the X1 Phase Can Continue the Reactions Steps to MA Product: The Alkoxide Route Mechanism*

Zhang-Lin et al. [12] performed a kinetic study of the oxidation of *n*-butane, butadiene, and furan catalyzed by

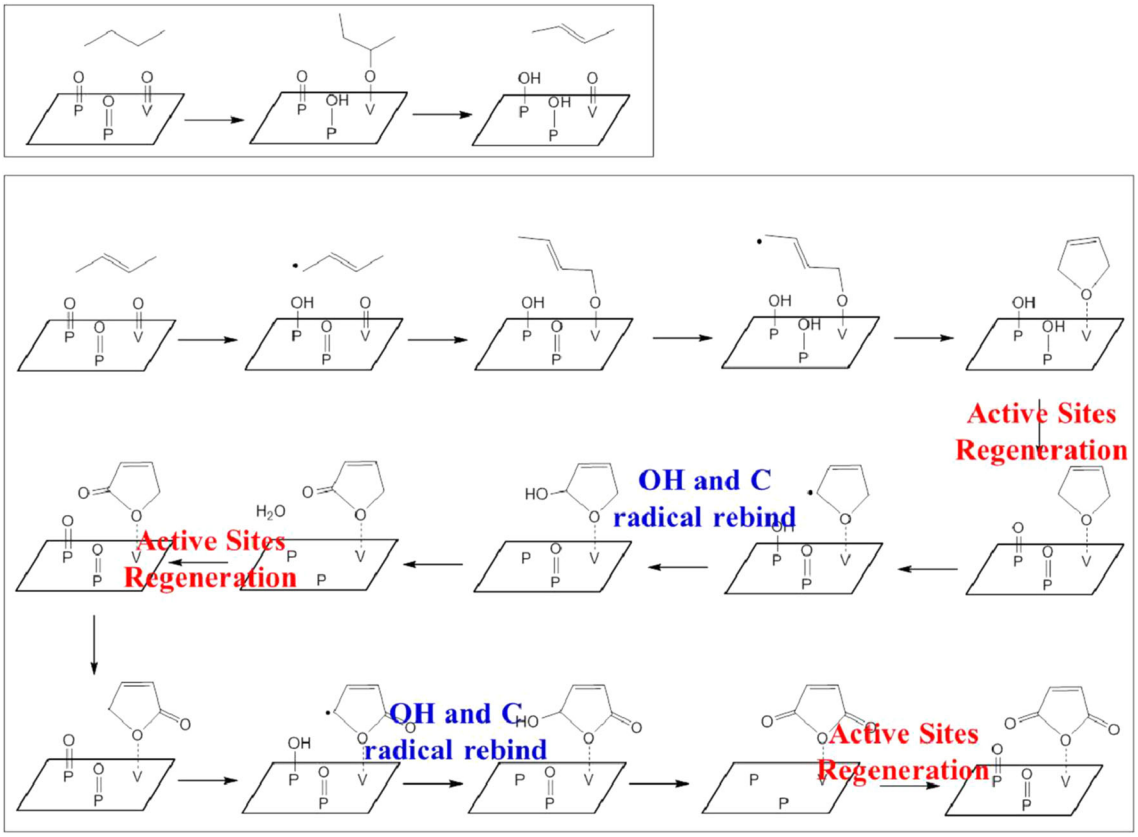

Fig. 20 DFT based mechanism following the alkoxide-route

VPO. By measuring the reactant conversion rate and MA formation rate from those oxidation reactions, they suggested a direct route from *n*-butane to MA. In this route, the activated *n*-butane forms an alkoxide intermediate on the surface and remains covalently bonded with the catalyst surface while all the subsequent oxidations step occur until the final MA product is released. Importantly, there is no desorption until the final product MA is formed.

Our version of this alkoxide route mechanism is in Fig. 20, where we depart from Zhang-Lin by assuming that butadiene can be formed, but reacts rapidly to form a bound 2,5-dihydrofuran. Key assumptions in our mechanism are shown in Fig. 21, namely:

- Hydrogen abstraction by O=P;
- Carbon radical rebound with OH;
- Hydrogen abstraction by HO–P.

In order to construct the potential energy surface of the proposed mechanism, we need the following information:

(1) the binding energy between O=P and a hydrogen atom,
(2) the binding energy between HO–P and a hydrogen atom to form H_2O,
(3) the energy cost to break off the OH bound to P, and

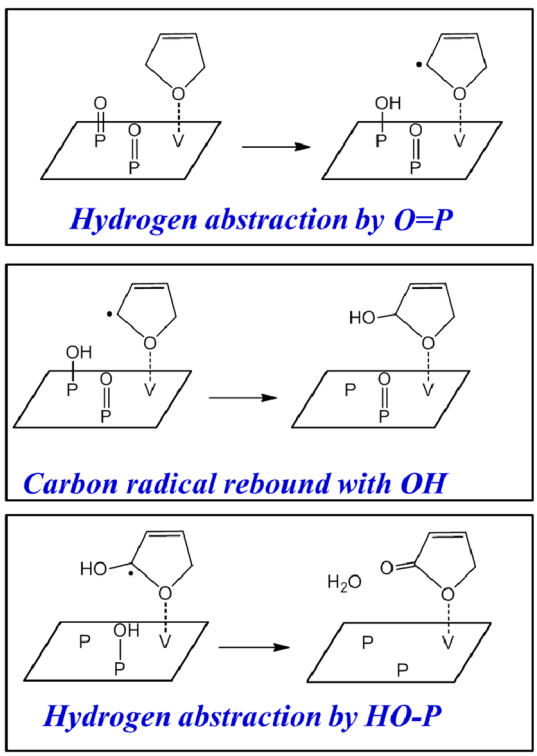

Fig. 21 Types of reactions involved in the alkoxide-route mechanism

(4) the C–H bond strength and C–OH bond strength of the cyclic intermediates.

Figure 22 uses a two layer model for QM calculations to determine the strength of the P–OH bond at the surface P. We find that the second layer plays a key role. Instead of leaving a radical on the surface P after removal of the O, the P radical reacts with the P=O bond of a subsurface P to form a pyrophosphate bond and reduces a V in the second layer bridged to the second layer P. As a result of this stabilization, the energy to break the OH from the top P is only 69.7 kcal/mol. It should be noted in this part of the study we used the PBE-D2 functional instead of PBE while other computational conditions are the same.

Figure 23 compares the energy for a surface P–OH bond to extract a H to form H_2O, while stabilizing the surface P as in Fig. 22. Here we see that forming the H–OH bond is exothermic by only 63.5 kcal/mol (compared to 119 kcal/mol for a free OH), so that surface P–OH is not expected to activate the alkane C–H bond (unless perhaps aided by allylic stabilization of the substrate). In addition we see that the surface V=O bond is not adequate to activate alkanes.

Figure 24 examines how the second layer can stabilize formation of a surface vacancy. This indicates that addition of O into the substrate is more likely to come from P=O rather than V=O. We missed this possibility in the discussions of the olefinic route mechanism, because we did not explicitly consider the role of the second layer. Thus the steps that assume the substrate R forms V–O–R bonds may instead involve P–O–R bonds.

Figure 25 compares these energetics from the two-layer model with the ones we obtained with the one-layer model. Comparing the vacancy formation energy from two-layer and one-layer models, we estimate that the strength of interlayer P–O–P bond as 59.0 kcal/mol and the V–O–V bond as 20.4 kcal/mol.

Figure 26 reports the various bond energies for reactions with the 2,5-dihydrofuran intermediate.

Combining these energetics together leads to the results in Fig. 27 for the various steps in the alkoxide route mechanism. We have not calculated barriers for these steps since the two layer periodic calculations are far more demanding. However, given that every step is exothermic

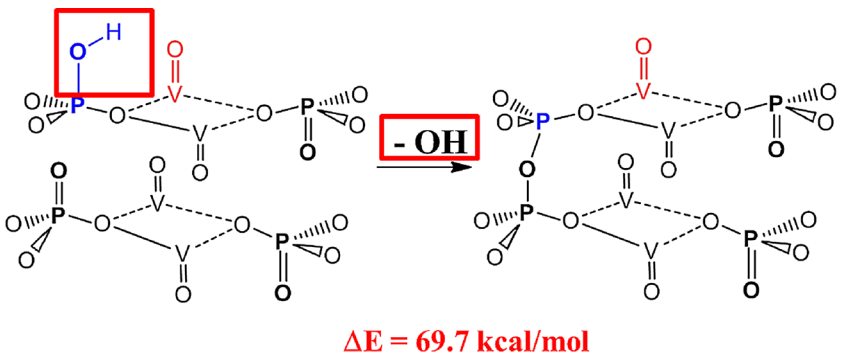

Fig. 22 Computed P–OH bond strength

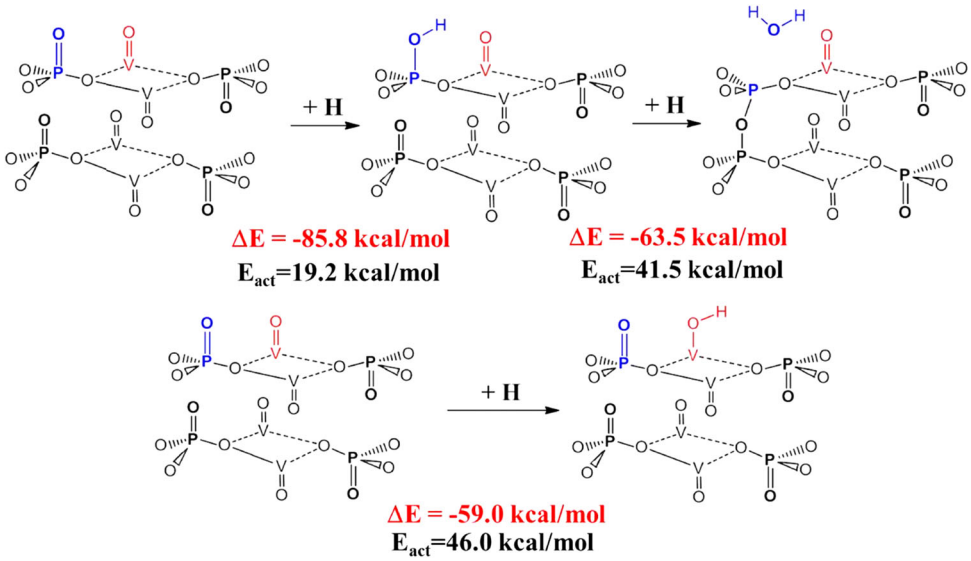

Fig. 23 Computed O–H bond formation energies (using the PBE-D2 functional)

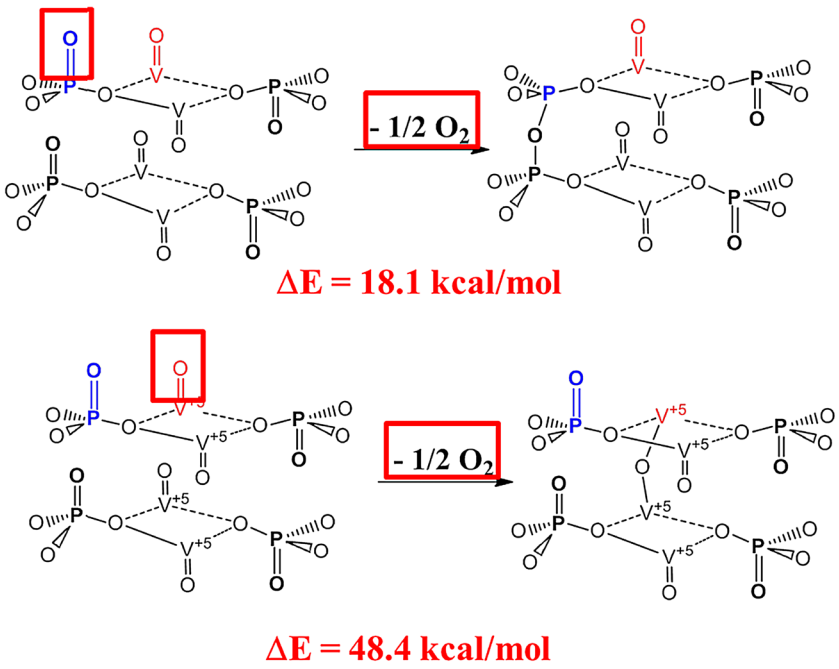

Fig. 24 Computed oxygen vacancy formation energies (two-layer model, PBE-D2)

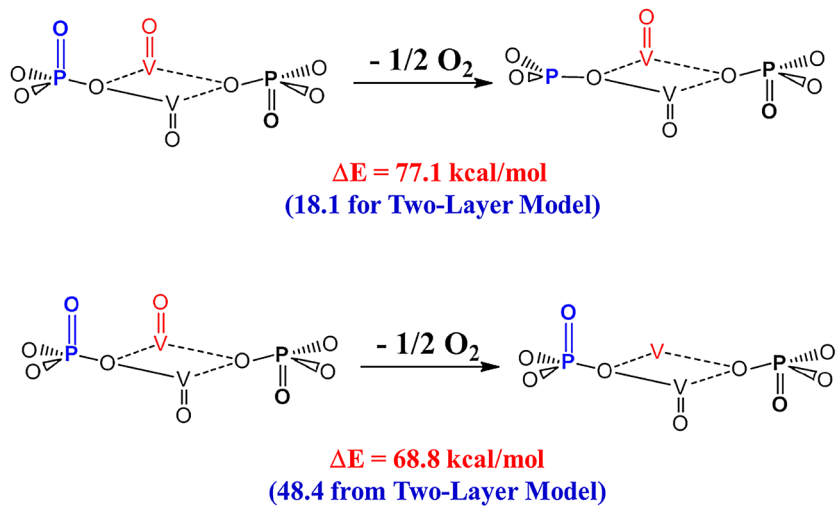

Fig. 25 Computed oxygen vacancy formation energies (one-layer model). Compared to the two-layer model, these results show that for the second layer, bonding decreases the energy to remove the O (for adding to the product) by 59.0 kcal/mol for O(1)=P and by 20.4 kcal for O(1)=V. This shows the importance of the layer structure for the catalysis (PBE-D2)

by 8–42 kcal/mol and the likely barriers are less than 20 kcal/mol for most steps, we consider that the alkoxide route is plausible with no major issues.

3.2.8 Summary of the ROA Mechanism for VPO Catalytic Selective Oxidation of Butane to MA

Summarizing, we used DFT to determine the reaction mechanism for *n*-butane oxidation to MA on VPO surfaces. In contrast to all previous suggestions, we found that surface O(1)=P (formed through the oxidation of pyrophosphate to two ortho-phosphates) is the site that activates *n*-butane (barrier of 13.5 kcal/mol). This high reactivity of O(1)=P is due to its relatively strong basicity coupled with the large reduction potentials of nearby V^{+5} ions.

We also demonstrated a full reaction pathway on this surface for oxidizing *n*-butane all the way to MA, with an overall barrier not exceeding 21.7 kcal/mol. This is consistent with the reaction proceeding at 673–723 K. Thus, we conclude the following critical elements of the VPO catalyst:

(1) We found that O(1)=P on the $VOPO_4$ surface is the active center for initiating the VPO chemistry, by extracting H from the alkane C–H bonds. This led our discovery of the *Reduction-Coupled Oxo Activation (ROA) mechanism.*

(2) We examined in detail two complete pathways for the subsequent functionalization of *n*-butane to MA and found the overall barrier to not exceed 21.7 kcal/mol.

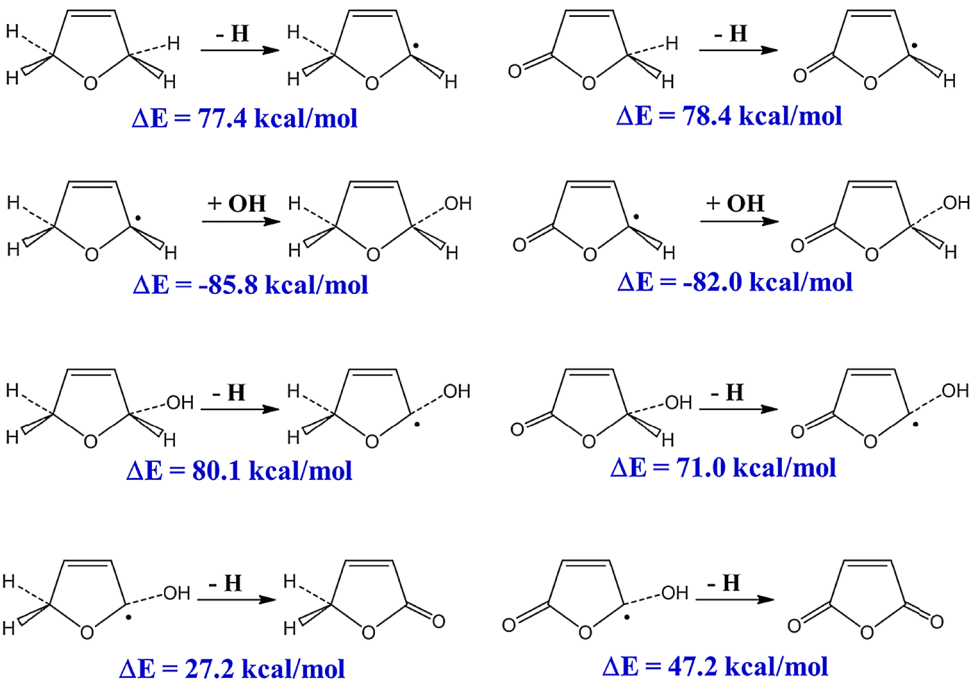

Fig. 26 C–H bond strength of the possible intermediates from DFT-PBE-D2

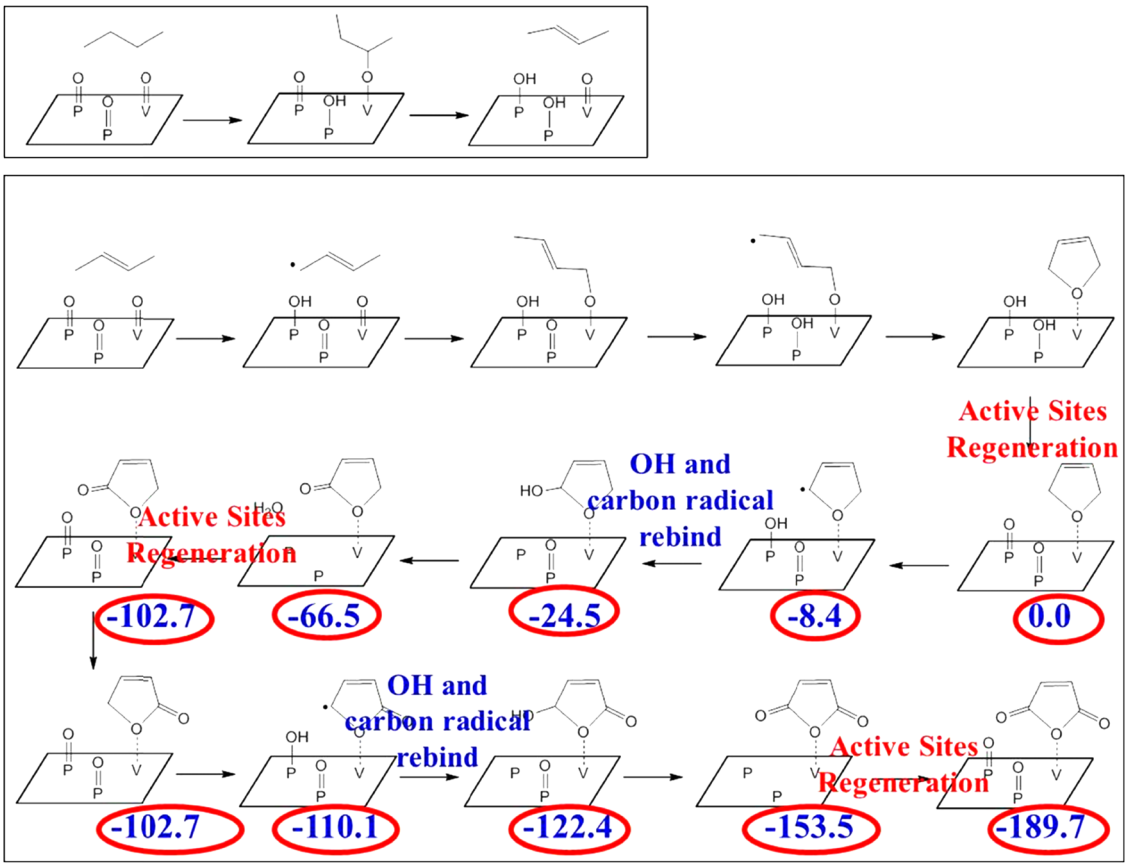

Fig. 27 DFT-PBE-calculated potential energy surface based on the alkoxide route mechanism. No activation energies have been calculated, but our experience indicates that they will be less than 23 kcal/mol, indicating that this mechanism is also compatible with experimental data

(3) We found that the second layer plays an essential important role in the chemistry. In reduced form the system forms P–O–P bridges which upon oxidation by gaseous O_2 generate the surface P=O bonds that activate the *n*-butane. Then as in Fig. 24, reforming the P–O–P bridges to the second layer activates the chemistry at the surface. Similarly, O–V–O bridges between the layers may play the role of converting a surface V^{3+} to a V^{4+}–O–V^{4+} bridge that activates a step at the surface.

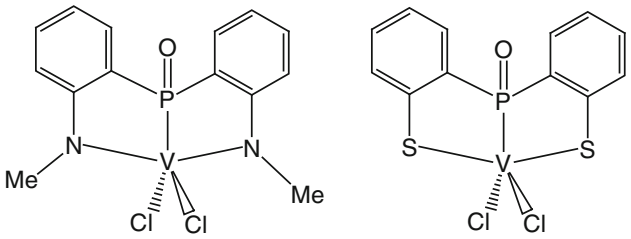

Fig. 28 Proposed organometallic complexes that activate the C–H bond of alkanes through the ROA mechanism [50]. We expect minimum activation energies of 22.4 and 13.3 kcal/mol for *n*-butane and calculate actual reaction barriers of 26.9 and 20.4 kcal/mol

4 Discussion

4.1 VPO Catalysis

We expect that these concepts learned from VPO chemistry may enable the design of new heterogeneous and homogeneous catalysts to activate alkane C–H bonds while functionalizing to form valuable organics.

Since pyrophosphates and phosphates are common components in heterogeneous catalysts, we speculate that they may play a key role for some of these catalytic systems as for the VPO system [45, 46].

Wachs et al. used in situ Raman spectroscopy to study the same oxidation using supported vanadia (V_2O_5) catalysts [38, 39]. They found that the addition of P_2O_5 phosphate additives increases the MA selectivity. Based on this observation they concluded that the V–O-P bond is the active site for the rate-determining-step. We agree with this conclusion, but we find more specifically that it is a O=P–O–V=O unit in which the phosphate is coupled through a bridging O to the V=O bond of V in +5 oxidization state. Also we find that it is the P=O bond that activates the C–H bond of *n*-butane, and not the V=O. It is not clear whether the P–O–P bonds of the additive are retained in the model catalyst. If they are, then we consider that Wachs' model system may operate under the same mechanism as we discovered for VPO. The activity would be expected to be less since the model system may not have the layer-to-layer integrity of the VPO catalyst. If the model catalyst does not retain the P–O–P units, then it may operate differently. Perhaps experimental tests would be to replace the P_2O_5 additive with PO_4.

4.2 Implications for Homogeneous Catalysts

Utilizing a non-metal oxo bond (such as P=O or S=O) to activate alkane C–H bonds would be ideal, since it would avoid the direct use of expensive metals at the active center [47]. Recently, this idea has been explored by Schwarz et al., [48] who used $[P_4O_{10}]^{\bullet+}$ to activate methane C–H bonds, and by de Petris et al. [49] who used $[SO_2]^{\bullet+}$ also to activate methane.

Indeed, we recently designed some homogeneous catalysts involving PO coupled directly to V (Fig. 28) that leads to very low barriers of 20 and 26 kcal/mol for dehydrogenation of butane [50].

4.3 Conclusion

These studies provide novel concepts for catalysis for both heterogeneous and homogeneous systems. They suggest that pyrophosphate or phosphate is catalytically important and is critical to the function of the current VPO system. Indeed it is likely to play a similar role in other heterogeneous systems. For example many selective oxidation catalysts involve P, As, Sb, Bi, Se, and Te, all which may activate the substrate by a similar mechanism. They also provide a new concept for designing catalysts that use non-metal oxo bonds instead of metal oxo bonds or metals for homogeneous alkane C–H activation.

Acknowledgments This work was supported mainly by NSF (CHE-1214158) but was initiated with support from the Center for Catalytic Hydrocarbon Functionalization, an Energy Frontier Reserch Center, DOE DE-SC0001298 with some additional support from Chevron USA Inc (Robert Sexton and Oleg Mironov).

References

1. Hodnett BK (2000) Heterogeneous catalytic oxidation. Wiley, New York
2. Ballarini N, Cavani F, Cortelli C, Ligi S, Pierelli F, Trifiro F, Fumagalli C, Mazzoni G, Monti T (2006) Top Catal 38:147
3. Centi G, Trifiro F, Ebner JR, Franchetti VM (1988) Chem Rev 88:55
4. Cheng MJ, Nielsen RJ, Tahir-Kheli J, Goddard WA III (2011) Phys Chem Chem Phys 13:9831
5. Thompson DJ, Fanning MO, Hodnett B (2003) J Mol Catal A 198:125
6. Haras A, Duarte HA, Salahub DR, Witko M (2002) Surf Sci 513:367

7. Robert V, Borshch SA, Bigot B (1997) J Mol Catal A 119:327
8. Schiott B, Jorgensen KA, Hoffmann R (1991) J Phys Chem 95:2297
9. Goddard III WA (1996) Recent developments in quantum mechanics and molecular dynamics with applications to problems in materials, catalysis, and biochemistry. In: Proceedings of 10th Institute for Fundamental Chemistry 11th symposium, Kyoto, Japan, May 1995, p 57
10. Gleaves JT, Ebner JR, Kuechler TC (1988) Catal Rev Sci Eng 30:49
11. Schuurman Y, Gleaves JT (1994) Ind Eng Chem Res 33:2935
12. Zhang-Lin Y, Forissier M, Sneeden RP, Vedrine JC, Volta JC (1994) J Catal 145:256
13. Chen B, Munson EJ (2002) J Am Chem Soc 124:1638
14. Coulston GW, Bare SR, Kung H, Birkeland K, Bethke GK, Harlow R, Herron N, Lee PL (1997) Science 275:191
15. Agaskar PA, Decaul L, Grasselli RK (1994) Catal Lett 23:339
16. Perdew JP, Burke K, Ernzerhof M (1996) Phys Rev Lett 77:3865
17. Vanderbilt D (1990) Phys Rev B 41:7892
18. Monkhorst HJ, Pack JD (1976) Phys Rev B 13:5188
19. Henkelman G, Jonsson H (2000) J Chem Phys 113:9978
20. Henkelman G, Uberuaga BP, Jonsson H (2000) J Chem Phys 113:9901
21. Saito T, Terashima T, Azuma M, Takano M, Goto T, Ohta H, Utsumi W, Bordet P, Johnston DC (2000) J Solid State Chem 153:124
22. Geupel S, Pilz K, van Smaalen S, Bullesfeld F, Prokofiev A, Assmus W (2002) Acta Crystallogr C 58:E10
23. Grimme S (2006) J Comput Chem 27:1787
24. Hehre WJ, Ditchfie R, Pople JA (1972) J Chem Phys 56:2257
25. Francl MM, Pietro WJ, Hehre WJ, Binkley JS, Gordon MS, Defrees DJ, Pople JA (1982) J Chem Phys 77:3654
26. Goddard WA III (1968) Phys Rev 174:659
27. Kahn LR, Goddard WA III (1968) Chem Phys Lett 2:667
28. Kahn LR, Goddard WA III (1972) J Chem Phys 56:2685
29. Melius CF, Goddard WA III (1974) Phys Rev A 10:1528
30. Melius CF, Olafson BD, Goddard WA III (1974) Chem Phys Lett 28:457
31. Hay PJ, Wadt WR (1985) J Chem Phys 82:299
32. Busca G, Centi G, Trifiro F, Lorenzelli V (1986) J Phys Chem 90:1337
33. Busca G, Cavani F, Centi G, Trifiro F (1986) J Catal 99:400
34. Cheng MJ, Goddard WA III (2013) J Am Chem Soc 135:4600
35. Chenoweth K, van Duin ACT, Persson P, Cheng MJ, Oxgaard J, Goddard WA III (2008) J Phys Chem C 112:14645
36. Kung HH (1986) Ind Eng Chem Prod Res Dev 25:171
37. Joly JP, Mehier C, Bere KE, Abon M (1998) Appl Catal A 169:55
38. Wachs IE, Jehng J-M, Deo G, Weckhuysen BM, Guliants VV, Benziger JB (1996) Catal Today 32:47
39. Wachs IE, Jehng J-M, Deo G, Weckhuysen BM, Guliants VV, Benziger JB, Sundaresan S (1997) J Catal 170:75
40. Volta JC (1996) Catal Today 32:29
41. Hutchings GJ, Desmartinchomel A, Olier R, Volta JC (1994) Nature 368:41
42. Shimoda T, Okuhara T, Misono M (1985) Bull Chem Soc Jpn 58:21630
43. Pepera MA, Callahan JL, Desmond MJ, Milberger EC, Blum PR, Bremer NJ (1985) J Am Chem Soc 107:4883
44. Kubias B, Rodemerck U, Zanthoff HW, Meisel M (1996) Catal Today 32:243
45. Alptekin GO, Herring AM, Williamson DL, Ohno TR, McCormick RL (1999) J Catal 181:104
46. Marcu IC, Sandulescu I, Millet JMM (2003) J Mol Catal A 203:241
47. Shilov AE, Shul'pin GB (1997) Chem Rev 97:2879
48. Dietl N, Engeser M, Schwarz H (2009) Angew Chem Int Ed Engl 48:4861
49. de Petris G, Troiani A, Rosi M, Angelini G, Ursini O (2009) Chem Eur J 15:4248
50. Cheng MJ, Fu R, Goddard WA III (2014) Chem Commun 50(2014):1748